Femtosecond laser surface structuring of silicon with Gaussian and optical vortex beams

Jijil JJ Nivas[a,b], Shutong He[a,c], Zhenming Song[d], Andrea Rubano[a,b], Antonio Vecchione[d], Domenico Paparo[e], Lorenzo Marrucci[a], Riccardo Bruzzese[a,b], Salvatore Amoruso[a,b]

[a] Dipartimento di Fisica, Università di Napoli Federico II, Complesso Universitario di Monte S. Angelo, Via Cintia, I-80126 Napoli, Italy

[b] CNR-SPIN, UOS Napoli, Complesso Universitario di Monte S. Angelo, Via Cintia, I-80126 Napoli, Italy

[c] Ultrafast Laser Laboratory, Key Laboratory of Opto-electronic Information Technical Science of Ministry of Education, College of Precision Instruments and Opto-electronics Engineering, Tianjin University, Tianjin 300072, P. R. China.

[d] Department of Physics, School of Science, Tianjin Polytechnic University, Binshuixi Road 399#, Xiqing District, Tianjin, 300387, P. R. China.

[e] CNR-SPIN, UOS Salerno, Via Giovanni Paolo II 132, I-84084 Fisciano, Italy

[f] National Research Council, Institute of Applied Science & Intelligent Systems (ISASI) 'E. Caianiello', Via Campi Flegrei 34, 80078 Pozzuoli (NA), Italy.

* Corresponding author. Tel.: +39 081 679287

E-mail address: amoruso@na.infn.it (S. Amoruso).

Abstract. We report an experimental analysis of femtosecond laser induced surface structuring of silicon by exploiting both Gaussian and Optical Vortex beams. In particular, we show how different surface patterns, consisting of quasi-periodic ripples and grooves, can be obtained by using different states of polarization offered by optical vortex beams. Both for Gaussian and optical vortex beams, an increase of the number of laser pulses, N, or beam energy, E_0, leads to a progressive predominance of the grooves coverage, with ripples confined in specific regions of the irradiated area at lower fluence. The average period of ripples and grooves shows a different dependence as a function of both E_0 and N, underlying important differences in mechanisms leading to the formation of ripples and grooves. In particular, our experimental characterization allows identifying a preliminary stage of grooves generation with rudimental surface structures, preferentially directed parallel to the laser polarization. This supports the idea that one possible mechanism of grooves formation lies in the progressive aggregation of clusters of nanoparticles densely decorating the ripples. Our experimental findings provide important indications on the basic understanding of the processes involved in laser surface structuring with ultrashort pulses that can guide the design of the surface patterns.

Keywords: Laser induced surface structures with Gaussian and Optical Vortex Beams; Femtosecond laser surface direct processing; Grooves

J. JJ Nivas, et al., Femtosecond laser surface structuring of silicon with Gaussian and optical vortex beams, Appl. Surf. Sci. 418 (2017) 565–571, http://dx.doi.org/10.1016/j.apsusc.2016.10.162

1. Introduction

In the field of femtosecond (fs) laser surface processing, the formation of quasi-periodic surface structures is a striking feature of increasing interest due to the crucial role played by the surface morphology in regulating several material properties [1–3]. The process of surface structures generation is boundary-less in terms of materials (metals, semiconductors and dielectrics), and shows interesting outlooks in the fabrication of functional surfaces, whose characteristics (e.g., optical, wetting, hydrophobic, sensing, contaminants or pathogens adhesion, and antimicrobial efficacy) depend on the peculiar nano- and micro-structure of the surface [4-11]. The features of the produced periodic surface structures vary with wavelength and polarization of the laser light and material properties. The typical quasi-periodic surface structures induced by fs laser pulse irradiation are generally indicated as *ripples* or (low-frequency) laser-induced periodic surface structures (LIPSS). The ripples are characterized by a sub-wavelength period and a preferential orientation. In metals and semiconductors, they are typically directed along the normal to laser polarization, meanwhile for dielectrics (fused silica and crystalline SiO_2, e.g.) a spatial disposition parallel to the laser polarization is observed [1, 12, 13]. Recently, the development of other, supervening quasi-periodic surface structures, named as *grooves*, was reported in semiconductors (Si and InP, e.g.) irradiated by a large number of laser pulses, and at higher fluence than ripples [14-20]. Grooves are microstructures with preferential orientation along laser polarization, and a period larger than laser wavelength. Moreover, all surface structures produced by fs laser structuring are always decorated with nanoparticles produced during the laser ablation process [1].

Several mechanisms have been considered for the formation of ripples on metals and semiconductors irradiated with fs pulses, which include inhomogeneous energy deposition due to the interference between the incident beam and a scattered interface field, excitation of surface plasmon polaritons (SPPs), self-organization of surface instabilities, hydrodynamics, etc. [see e.g. Refs. 1-3 and papers therein quoted]. However, no widespread consensus has been reached yet on the mechanism leading to ripples formation [1,21], while grooves generation attracted more interest only very recently [14-16]. In this respect, silicon is often the case study material, since it shows all kinds of surface structures and presents always interest because of its usefulness in electronic industry.

Here, we report an experimental study of the surface structures produced on a crystalline silicon target irradiated, in air, with Gaussian and Optical Vortex (OV) beams with fs pulse duration. OV are light beams carrying Orbital Angular Momentum characterized by a helical wave-front and controllable polarization patterns [22,23], that can offer the possibility of generating more complex surface structures [24-30]. Our experimental findings suggest that the use of fs OV beams allows one to further extend the possibilities offered by the more standard Gaussian beam approach in tailoring the morphological features of the surface structures.

2. Experimental methods

The fs laser pulses are provided by a regenerative Ti:Sapphire amplifier delivering linearly polarized pulses with ≈35 fs duration at a central wavelength of 800 nm. A combination of half wave-plate and polarizer was used to control the pulse energy. Experiments were carried out with Gaussian and OV beams. The beam with a Gaussian spatial intensity profile is provided by the fundamental output of the laser source. The OV beam is generated by exploiting an efficient beam converter based on a *q-plate* with a topological charge $q = +1/2$ through spin-to-orbital conversion of the angular momentum of light [22]. After the *q-plate*, the spatial intensity distribution of the beam presents a central region of zero intensity (due to undefined phase on the beam axis), a principal intense ring and

several secondary rings at increasing radial distance from the axis [23]. The central part of this beam is spatially filtered with an iris, thus obtaining an OV beam with an annular spatial profile. The beam is focused on the target by a plano-convex lens with a 75 mm focal length, in ambient air. The single-crystalline (100) silicon target is mounted on a XY-translation stage and located perpendicular to the laser beam direction. The desired number of laser pulses, N, is applied to the same spot on the target surface by means of an electromechanical shutter. The target surface morphology is analyzed by using a field emission scanning electron microscope. The SEM images are typically registered through secondary electrons (SE) detection, but in some cases images with higher contrast are also obtained by using an In-Lens (IL) detector located inside the electron column of the microscope and arranged rotationally symmetric around its axis.

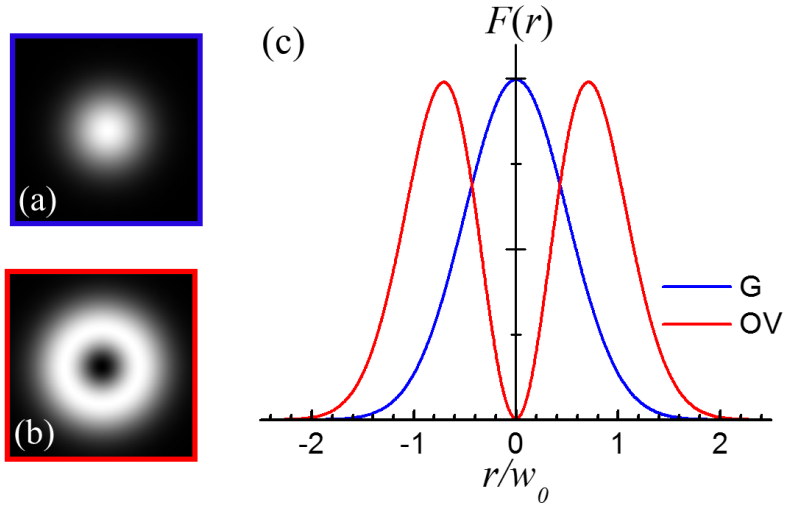

Figure 1. Spatial profiles of (a) Gaussian and (b) OV beams characterized by the same value of the peak fluence F_p and waist w_0. (c) Normalized spatial profiles of the Gaussian and OV pulse fluence $F(r)$ along the diameter of the beam (in units of the beam waist w_0). G and OV refer to the Gaussian and OV beams, respectively.

The spatial profile of the Gaussian and OV beams irradiating the target surface are schematically shown in panels (a) and (b) of Fig. 1, respectively. The Gaussian beam is linearly polarized and its polarization direction can be controlled by means of a half wave-plate. The OV beam is characterized by an annular spatial profile and its state of polarization (SoP) is manipulated by appropriate rotation of the linear polarization of the Gaussian beam entering the q-plate with respect to its optical axis. This beam converter allows the generation of azimuthal, radial and spiral SoP. Fig. 1(c) reports the spatial profiles of the pulse fluence $F(r)$ for the Gaussian and OV beams, r being the spatial coordinate along the diameter, which are described as:

$$F_G(r) = \frac{2E_0}{\pi w_0^2} exp\left[-\frac{2r^2}{w_0^2}\right] \quad (1)$$

and

$$F_{OV}(r) = \frac{2^2 E_0}{\pi w_0^4} r^2 \exp\left[-\frac{2r^2}{w_0^2}\right] \quad (2)$$

where E_0 is the beam energy, w_0 the waist of the fundamental Gaussian beam [22], and the subscripts G and OV refer to Gaussian and OV beams, respectively. The Gaussian beam fluence profile $F_G(r)$ presents a peak value $F_{G,p} = 2E_0/\pi w_0^2$ at r=0 and reduces to $1/e^2$ of the peak value at r=w_0. Instead, the fluence profile $F_{OV}(r)$ of the OV beam is null at center and shows a peak value $F_{OV,p} = 2e^{-1}E_0/\pi w_0^2 \approx 0.74\,E_0/\pi w_0^2$ at a radial distance $r_p = w_0/\sqrt{2}$ from the center. Moreover, the fluence reduces to $1/e^2$ of the peak value at two different locations on the two sides of the peak, namely at r_{in}≈0.16 w_0 and r_{out}≈0.15 w_0, due to the dissimilar fluence spatial gradient in the central ($r < r_p$) and external ($r > r_p$) regions of the OV beam profile.

3. Results and discussion

In the following, we first illustrate the typical morphological features developed on the surface irradiated by Gaussian and OV beams. Then, we analyze the relative prominence of the two surface structures in the irradiated area, as well as the variation of the typical spatial period of ripples and grooves, as a function of the pulse energy, E_0, and number of pulses, N. Finally, we discuss a physical mechanism interpreting the grooves generation as due to a progressive aggregation and melting of nanoparticles assemblies decorating the surface structures.

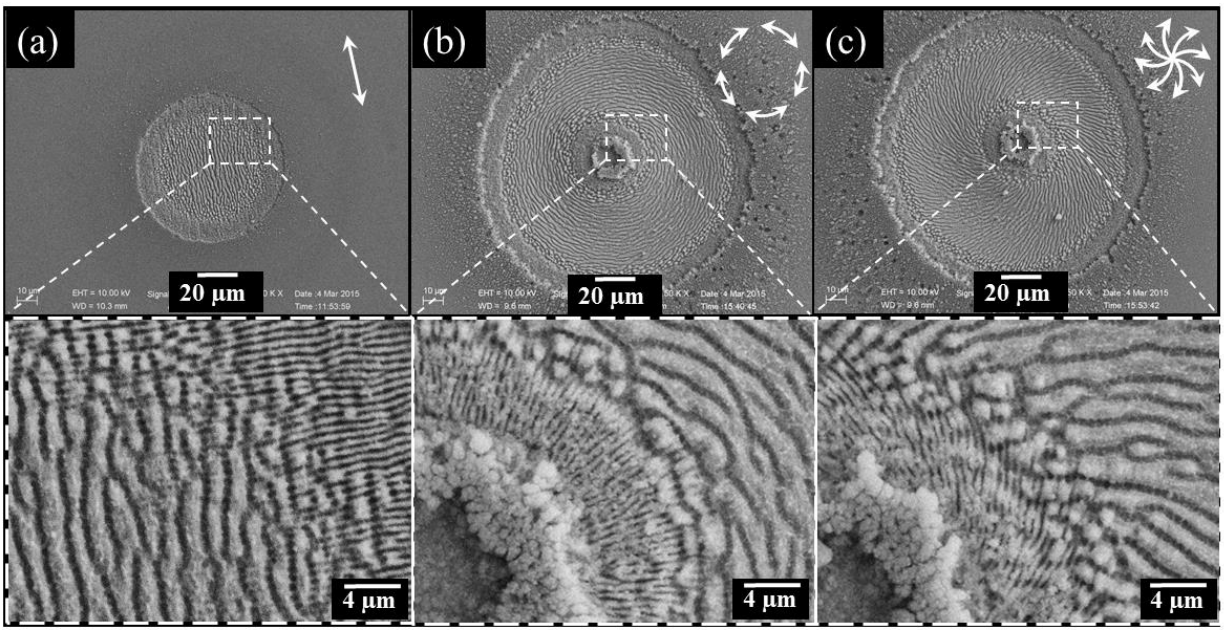

Figure 2. Examples of the surface structures developed on the silicon target after irradiation with N = 100 pulses: (a) Gaussian beam with linear polarization; (b) OV beam with azimuthal SoP; (c) OV beam with spiral SoP. The

lower panels are zoomed views on the areas indicated by the white boxes illustrating finer details of the surface texture. The different SoP of the beams are indicated by the white arrows.

Fig. 2 reports typical examples of the surface structures produced on the silicon target after irradiation with N=100 laser shots with a linearly polarized Gaussian beam (panel (a)) and OV beams with an azimuthal (panel (b)) and spiral (panel (c)) SoP. The lower panels in Fig. 2 reports zoomed views on the areas indicated by the white boxes illustrating finer details of the surface texture. In Fig. 2, the different SoP of the beams are indicated by the white arrows. The experimental conditions correspond to Gaussian and OV beams with comparable values of the peak fluence F_p (≈0.5 J/cm^2) and waist w_0 (≈45 μm). The SEM images show the formation of shallow craters reflecting the beam shape. One can clearly observe the different spatial extension of the crater, which is smaller for the Gaussian beam than for the OV beam with rather similar parameters as a consequence of the different spatial profile of the laser pulse fluence $F(r)$ (see Fig. 1, e.g.). In particular, in both cases the external radii correspond to a fluence value of ≈0.1 J/cm^2 suggesting the same threshold fluence for ablation with N=100 pulses both for the Gaussian and OV beams, as indeed expected. Moreover, this also agrees fairly well with the fluence value at the inner radius (≈10 μm) of the OV beam corresponding to the central part of the beam with a fluence below the target ablation threshold. This area of the target surface is decorated by a circular structure formed by a large number of nanoparticles. In all cases, the presence of a dense layer of nanoparticles is also observed in the region adjoining the outer boundary of the ablated area.

The SEM images of Fig. 2 evidence a complex surface morphology. Two main regions can be recognized in the crater produced by the Gaussian beam (Fig. 2(a)) with a central area decorated by micro-grooves surrounded by a peripheral annulus with sub-wavelength ripples. These two regions are separated by a sharp ring showing rudiments of grooves situated above the underlying ripples. For the OV beams, the crater (Fig. 2, panels (b) and (c)) shows various annular regions characterized by different surface textures. Going from the center to the periphery, after the central region decorated by a large number of nanoparticles ($r \leq 10$ μm), one can observe a thin annulus of ripples with a width of ≈7 nm, a central ring of micro-grooves extending over ≈40 nm and finally a second, annular rippled region with a thickness of ≈8 nm. This, in turn, suggests that the various surface structures closely depend on the local fluence level, with grooves developing in the more intense area and ripples confined in the lower intensity tails of the fluence spatial distribution. Interestingly, Fig. 2 reports two examples of the surface patterns obtained by means of OV beams with an azimuthal (Fig. 2(b)) and spiral (Fig. 2(c)) SoP. Other patterns can be obtained by appropriate tuning of the beam converter. This clearly demonstrates that the use of OV beams offers the possibility to tailor the directionality of the quasi-periodic patterns of ripples and grooves through an appropriate selection of their SoP.

To illustrate the relative prominence of the two different surface structures (ripples and grooves), we analyze the dependence of the width of the different regions recognized in the ablation craters for both kind of beams (see Fig. 2, e.g.) as a function of the pulse energy, E_0, and number of pulses, N. In particular, as shown in the left part of Fig. 3, we consider the widths of the various areas corresponding to ripples (w_r) and grooves (w_g) for the Gaussian beam (upper SEM image), and internal ($w_{r,in}$) and external rings ($w_{r,ex}$) with ripples and central annulus with grooves (w_g) for the OV beam (lower SEM image). The variation of these widths with E_0 and N are reported in the right part of Fig. 3. The error bars indicate the uncertainty estimated by considering the variability in the recognition of the width

of the various regions obtained in repeated measurements by different individuals in our team. We notice that the lower image in the left part of Fig. 3 refers to an azimuthal SoP of the OV beam, but it is representative also for the other SoP since the variation of the various widths is found to be rather independent of the specific polarization in our weak focusing experimental conditions.

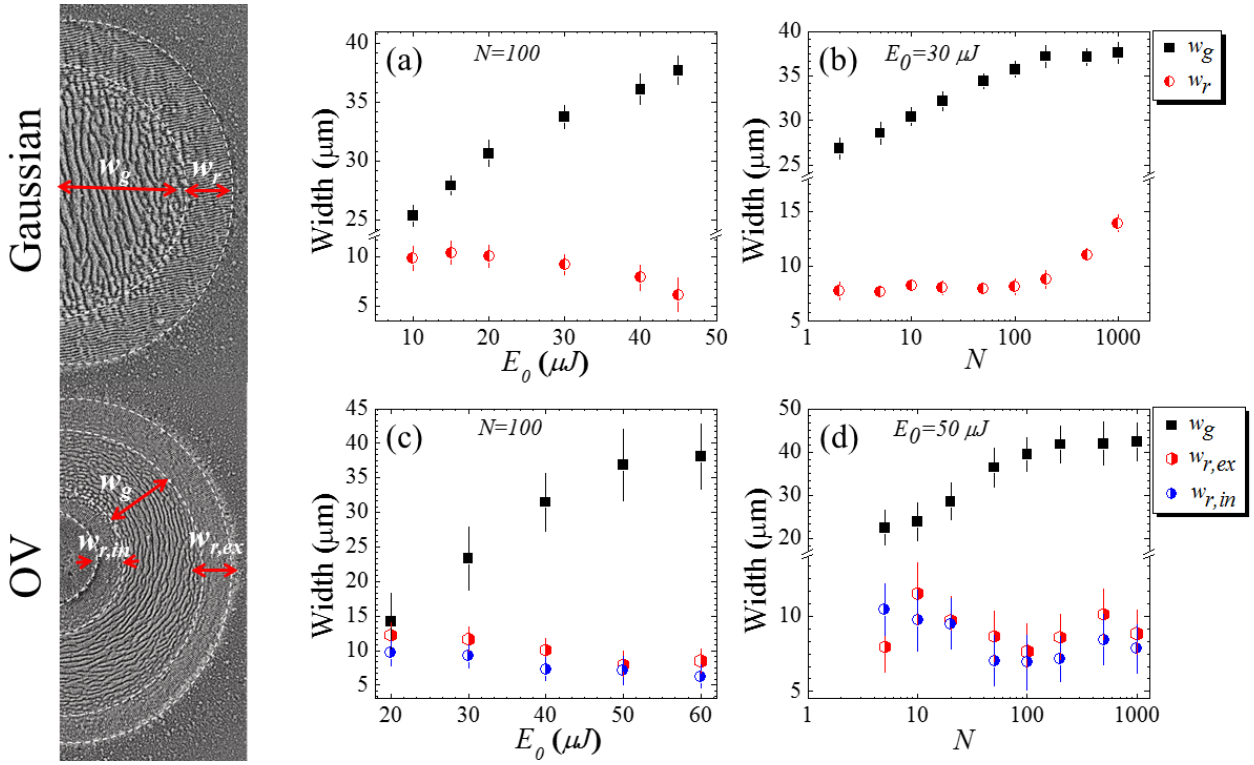

Figure 3. Variation of the width of the different structured surface regions recognized in the craters produced by irradiation with Gaussian and OV beams as a function of the laser pulse energy, E_0, and laser pulse number, N. Left part: zoomed views of SEM images corresponding to a portion of the crater generated by a Gaussian (upper panel) and OV (lower panel) beams, respectively. In each image, the widths of the various areas corresponding to rippled (w_r) and grooved (w_g) regions of the Gaussian beam, and internal ($w_{r,in}$) and external ($w_{r,ex}$) rippled and central grooved (w_g) annuli of the OV beams are indicated. Right part: variation of the widths as a function of E_0 and N for Gaussian ((a) and (b)) and OV ((c) and (d)) beams.

Considering first the energy variation reported in panels (a) and (c) of Fig. 3, the widths w_r, $w_{r,in}$ and $w_{r,ex}$ of the annular regions decorated with ripples present a weak dependence on the pulse energy E_0 for both beams, with a slight tendency to reduce as E_0 increases. Instead, in both cases the extension of the grooved area, w_g, is an increasing function of the pulse energy E_0. The observed trend is consistent with the fact that the overall size of the ablation crater increases with the pulse energy, E_0, both for Gaussian and OV beams [31, 32]. In particular, as E_0 increases the area decorated by the grooves rises accordingly as a consequence of the fact that the region of the beam with a fluence larger than the threshold value for grooves formation progressively extends over a larger area. Moreover, ripples remain confined in zones of the beam at lower fluence (between thresholds values for grooves formation

and target ablation), thus leading to the observed weak dependence of the thickness of the rippled regions (i.e. w_r, $w_{r,in}$ and $w_{r,ex}$) on E_0.

As for the variation with the number of pulses N, panels (b) and (d) of Fig. 3 show that w_g also increases with N, eventually tending to level off at high number of pulses, both for the Gaussian and OV beams. This condition typically corresponds to the progressive formation of a deeper ablation crater. As for ripples, in the case of the OV beam (Fig. 3, panel (d)), the thickness of the rippled areas does not show a monotonous trend and the values of $w_{r,in}$ and $w_{r,ex}$ are rather scattered. It is worth observing that the scattering of the $w_{r,in}$ and $w_{r,ex}$ values is due to the presence of a blurred transitional region between ripples and grooves, which somehow limit a distinct identification of their separation. Nevertheless, the limited variation within a narrow range of values of the order of 10 μm suggests a weak dependence of $w_{r,in}$ and $w_{r,ex}$ on N. A similar, almost stationary dependence on N occurs for w_r in the case of the Gaussian beam (Fig. 3, panel (b)) for $N \leq 200$. At larger N this trend is, then, followed by a gradual increase of w_r with N, which is likely related to both the progressive reduction of the fluence threshold for ablation associated to the accumulation effects described by incubation behavior [17,24] and the observed levelling off of the width of the grooved region.

The dependence of the spatial period of ripples, Λ_r, and grooves, Λ_g, on laser pulse energy E_0 and number of pulses N is reported in Figure 4 both for the Gaussian (panels (a) and (c)) and OV (panels (b) and (d)) beams, respectively. The period of the surface structures slightly changes with location, therefore Fig. 4 reports the average value of the period and its variability is shown as an error bar.

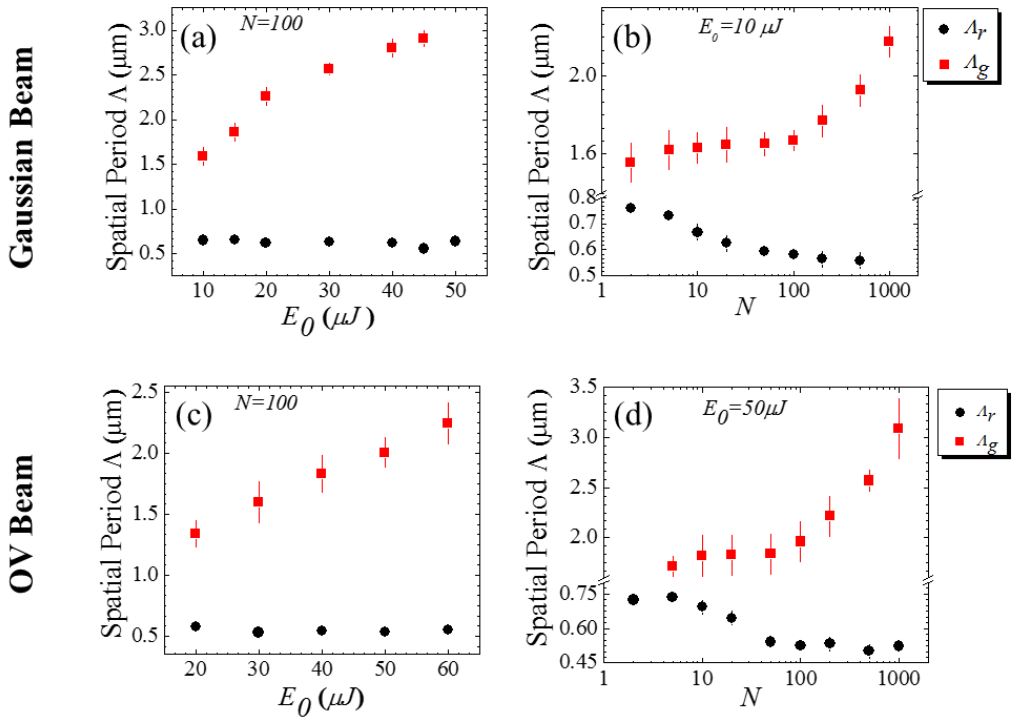

J. JJ Nivas, et al., Femtosecond laser surface structuring of silicon with Gaussian and optical vortex beams, Appl. Surf. Sci. 418 (2017) 565–571, http://dx.doi.org/10.1016/j.apsusc.2016.10.162

Figure 4. Variation of the spatial period of ripples, Λ_r, and grooves, Λ_g, as a function of the laser pulse energy E_0, for (a) Gaussian and (c) OV beams, at N = 100 pulses. Variation of Λ_r and grooves, Λ_g, as function of the number of pulses N for (b) Gaussian beam, at E_0=10 μJ, and for (d) OV beam, at E_0=50 μJ.

Considering first the sub-wavelength ripples, Fig. 4 shows a noticeable effect of N (Fig 4, panels (b) and (d)) and a rather weak influence of E_0 (Fig. 4 panels (a) and (c)) on Λ_r, for both cases. Previous analyses on energy variation are limited to few values [30]. Here we observe that the average ripple period remains almost constant over a rather broad range of pulse energies, for both Gaussian and OV beams. This can be rationalized by considering that an increase of E_0 results in a rise of the local fluence value over the irradiated region. As observed in Fig. 3, the conditions for ripples formation are generally fulfilled only in the outer areas of the beam profile characterized by lower values of the fluence. As a consequence, the range of local fluence values where ripples can form remains almost unchanged as the pulse energy varies, thus leading to the observed weak dependence of the average ripple period Λ_r on E_0. Instead, in the regions of higher fluence the presence of grooves develops, whose period variation on N and E_0 is reported in Fig. 4 and discussed below. On the other hand, Λ_r progressively decreases for $10 < N < 100$, then reaching a stationary regime for larger N. The decreasing variation of Λ_r with N has been addressed earlier as a general characteristics of the ripples formation processes [15, 17, 33-35]. Interestingly, we observe that the reduction with N is then followed by a plateau at large number of pulses, suggesting a progressive saturation at a large number of laser pulses. In the frame of an interpretative scenario based on the SPP-assisted ripples formation, $\Lambda_r = \lambda_{las}/\mathrm{Re}[\eta]$ where λ_{las} and η are the laser wavelength and the effective refractive index of the excited target surface, respectively [1]. Huang et al. propose the concurrence of two different mechanisms to explain the reduction of Λ_r on N: the field effect and the grating-assisted SPP coupling [33]. The former mechanisms is related to the progressive confinement of the ripples to regions of the beam periphery characterized by a progressive lowering of the local fluence, as N increases. This, in turn, results in a decrease of the excited carriers local density with an associated increase of $\mathrm{Re}[\eta]$ and a consequent reduction of the ripple period [15,33]. The latter considers the fact that, as N increases, the ripples becomes gradually deeper with a reduction of the SPP periodicity and a consequent decrease of Λ to satisfy the appropriate condition of optimal coupling. However, it is worth noticing that an alternative dynamic model proposed by Reif et al. rationalizes the formation and evolution of the produced surface structures on the base of a self-organization process [36]. In this case, the variation of the structures morphological features are associated to an increase of the irradiation dose with N.

The spatial period of grooves Λ_g shows an increasing dependence on both N and E_0. Our experimental findings on the variation of Λ_g with N is in agreement with other recent experimental observations [15], addressing an approximately linear rise of the grooves period with N during irradiation of silicon with a Gaussian beam (≈470 fs, 800 nm) at an average laser fluence of 0.7 J/cm^2. However, in this study the analysis was limited to $20 < N < 100$. Here, we observe that, for the Gaussian beam, the increasing trend of Λ_g on N continues up to N as high as 1000 (see Fig. 4(c)) and it also holds for the OV beam, thus suggesting it as a general characteristic of the grooves generated during laser irradiation of silicon with ultrashort pulses. Moreover, Fig. 4(a) and 4(c) show that the grooves period also increases with the pulse energy E_0, in the investigated range.

The supra-wavelength dimension and the diverse dependence of the grooves period on number of pulses and energy suggest that mechanisms of their formation are different with respect to ripples. Fig. 5 reports examples of

SEM images illustrating the surface texture in various areas of the irradiated surface, which allows gaining clues about some interesting aspects involved in the grooves generation. The SEM micrograph of Fig. 5(a) shows a characteristic image of the sub-wavelength ripples, oriented along the normal to laser polarization, registered with SE detector. It shows that the target surface is characterized by an extensive and dense coverage of nanoparticles, as typical for fs laser ablation [1, 37, 38]. Such an effect is still more prominent for ablation in air, due to a stronger backward flux of ablated material towards the target surface [38]. Fig. 5(b) reports a zoomed view of the ripples registered by using the IL detector, which provides more defined surface details than standard SE detector. This image clearly evidences the presence of large assemblies of nanoparticles located over underlying ripples. Figs. 5(c) and 5(d) reports SEM images on the intermediate region between ripples and grooves and of an area where grooves are fully developed, respectively, acquired with the IL detector. In Fig. 5(c), various rudiments of grooves are recognized (indicated by yellow arrows), which bridge over some underlying ripples and are preferentially elongated in the direction of the laser polarization. In particular, the one indicated by the larger arrow in Fig. 5(c) presents a morphology rather similar to that of the fully developed grooves shown in Fig. 5(d). The grooves are in form of stripes covering the underlying ripples and are aligned along the laser polarization. The structures evidenced in Fig. 5(c) seem small, primary rudimental constituents outlining an earlier stage of the grooves formation process, thus suggesting that the grooves form above the ripples as a result of the progressive aggregation of various, large clusters of nanoparticles. In particular, the smooth central part of the grooves suggests that their formation mechanisms possibly involve melting and re-solidification of the clusters of nanoparticles. Finally, an increase of the energy E_0 and number of pulses N can likely favor aggregation of rudimental grooves structures thus leading to the progressive rise of the average grooves period (see Fig. 4).

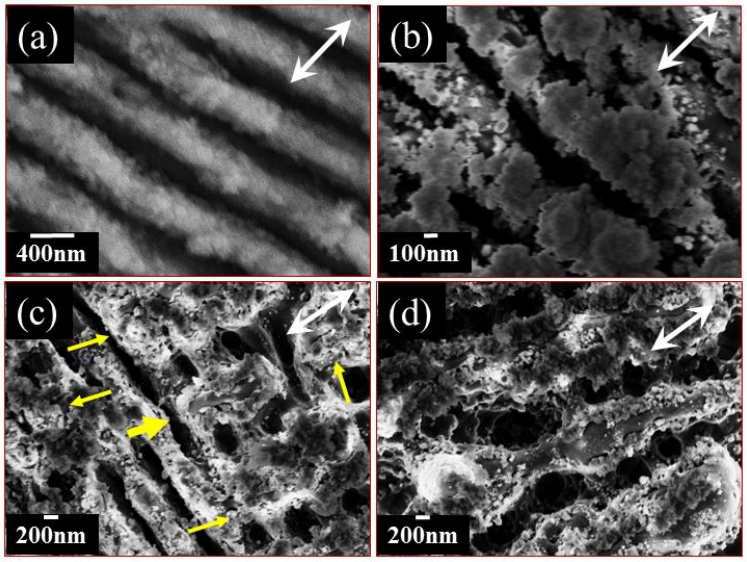

Figure 5. SEM images illustrating the typical morphological features of the surface structures. (a) SEM image of the ripples registered with SE detector; (b) zoomed view of the ripples registered with IL detector showing assemblies of nanoparticles decorating underlying ripples; (c) SEM image of the intermediate region between ripples and grooves registered with IL detector. The yellow arrows point to rudiments of grooves covering the

underlying ripples and directed along the laser polarization. (d) SEM image of the grooves registered with IL detector. In all panels, the direction of the incident laser polarization is reported as a white double-headed arrow.

Detailed analyses on the grooves generation mechanisms are still rather scarce. Varlamova et al. [19,20] attributed their formation to a stage of the evolution of the surface structures characterized by some type of coagulation/aggregation mechanisms in the frame of a self-organization, non-linear dynamical model that evidences the progressive generation such supra-wavelength features for larger irradiation dose. Instead, Tsibidis et al. [15], proposed a hybrid model complementing the electromagnetic interference effects with melt hydrodynamics, which predicts the formation of grooves, whose spatial period varies approximately linearly with the number of pulses for $20 \leq N \leq 100$, for a fs laser pulse with a Gaussian intensity profile. Such last study only addressed the role of N, while the effect of the pulse energy on the grooves period was not considered. Our experimental findings suggest an almost linear scaling of the grooves period with both E_0 and N (even for N as high as 1000), thus addressing the importance of the global excitation level in the grooves formation and evolution dynamics. Moreover, they point out an interesting influence of the progressive coagulation of nanoparticles as a further possible mechanisms of grooves generation. Preliminary findings obtained in multi-pulse experiment carried out in air and high vacuum seems to support the key role played by nanoparticles, since the irradiated surface displays a different morphology as a consequence of the diverse level of nanoparticles decoration of the rippled surface in the two conditions. This aspect will be subject of future communications.

5. Summary

We have experimentally investigated the process of fs laser surface structuring of silicon with both Gaussian and OV beams, in air. The different spatial profiles of two beams allow evidencing that the surface develops a texture that depends on the local value of the laser pulse fluence and number of laser pulses, as well as on the local SoP. Sub-wavelength ripples, aligned along a direction normal to the laser polarization, mainly forms in peripheral regions of the beam characterized by low fluence, while supra-wavelength grooves, preferentially directed along the local laser polarization, are generated in the region of higher fluence. Moreover, an increase of either the number of laser pulses, N, or beam energy, E_0, results in a progressive rise of the grooved region within the irradiated area.

The ripples period shows a weak dependence on laser pulse energy, while reducing progressively with number of pulses, N, in agreement with previous reports [15, 17, 33-35], then reaching a stationary regime at larger N values. On the contrary, the period of the grooves is an increasing function of both N and E_0. This suggests that the mechanisms of grooves generation are different from those underlying the ripples formation. Our experimental characterization of the surface structures identify rudimental surface structures preferentially directed parallel to the laser polarization. These seem to result from a progressive aggregation of nanoparticles and clusters of nanoparticles, generated during the ablation and densely decorating the ripples, in the regions of higher fluence level, that eventually give rise to the creation of grooves. To further support this scenario, we are carrying out experiments by limiting the nanoparticle re-deposition, and preliminary results suggest a correlated reduction of the grooves formation efficiency. Such results will be subject of a forthcoming report.

Finally, the simultaneous analysis of the surface structures produced by fs pulse with Gaussian and OV spatial profile singles out the possibility to generate a variety of surface structures by controlling the directionality of the quasi-periodic patterns of ripples and grooves through an appropriate selection of SoP, energy and number of laser pulses. While our investigation with the OV beam was limited to the SoP generated by exploiting a beam converter

based on a q-plate with a topological charge $q = + 1/2$, preliminary results with higher values of q indicate that OV beams with even more complex SoP can be created and further enhance the variety of surface micro-structures that can be fabricated. As formation of quasi-periodic surface structures seems to be ubiquitous to laser irradiation of solid targets with ultrashort pulses, the method can be directly extended to other materials of interest. These findings can provide important clues on the basic understanding of the processes involved in direct surface processing with ultrashort pulses, as well as guiding the implementation of surface structures of applicative interest.

Acknowledgements

A.R. acknowledges funding from the European Union (Programme FP7-PEOPLE-2012-CIG, Grant Agreement No. PCIG12-GA-2012-326499-FOXIDUET). Z.S. thanks the Tianjin Municipal Education Commission for providing his scholarship grant. This work was supported by the European Research Council (ERC), under grant no. 694683 (PHOSPhOR).

References

[1] A.Y. Vorobyev, C. Guo, Direct femtosecond laser surface nano/microstructuring and its applications, Laser Photon. Rev. 7 (2013) 385–407.

[2] K. Sugioka, Y. Cheng, Ultrafast lasers—reliable tools for advanced materials processing, Light Sci. Appl. 3 (2014) e149.

[3] T.-H. Her, in Comprehensive Nanoscience and Technology, D. Andrews, G. Scholes, and G. Wiederrecht, eds. (Elsevier, 2011), Chap. 4.10.

[4] A.Y. Vorobyev, C. Guo, Colorizing metals with femtosecond laser pulses, Appl. Phys. Lett. 92 (2008) 041914.

[5] S. Moradi, S. Kamal, P. Englezos, S.G. Hatzikiriakos, Femtosecond laser irradiation of metallic surfaces: effects of laser parameters on superhydrophobicity, Nanotech. 24 (2013) 415302.

[6] Y.-L. Zhang, H. Xia, E. Kim, H.-B. Sun, Recent developments in superhydrophobic surfaces with unique structural and functional properties, Soft Matter. 8 (2012) 11217–11231.

[7] V. Zorba, L. Persano, D. Pisignano, A. Athanassiou, E. Stratakis, R. Cingolani, et al., Making silicon hydrophobic: wettability control by two-lengthscale simultaneous patterning with femtosecond laser irradiation, Nanotech. 17 (2006) 3234.

[8] A.Y. Vorobyev, C. Guo, Direct creation of black silicon using femtosecond laser pulses, Appl. Surf. Sci. 257 (2011) 7291–7294.

[9] H. Huang, L.-M. Yang, S. Bai, J. Liu, Blackening of metals using femtosecond fiber laser, Appl. Opt. 54 (2015) 324–333.

[10] M. Halbwax, T. Sarnet, P. Delaporte, M. Sentis, H. Etienne, F. Torregrosa, et al., Micro and nano-structuration of silicon by femtosecond laser: application to silicon photovoltaic cells fabrication, Thin Solid Films. 516 (2008) 6791–6795.

[11] S. Zoppel, H. Huber, G.A. Reider, Selective ablation of thin Mo and TCO films with femtosecond laser pulses for structuring thin film solar cells, Appl. Phys. A. 89 (2007) 161–163.

J. JJ Nivas, et al., Femtosecond laser surface structuring of silicon with Gaussian and optical vortex beams, Appl. Surf. Sci. 418 (2017) 565–571, http://dx.doi.org/10.1016/j.apsusc.2016.10.162

[12] S. Höhm, A. Rosenfeld, J. Krüger, J. Bonse, Femtosecond laser-induced periodic surface structures on silica, Journal of Applied Physics 112, 014901 (2012),

[13] S. Höhm, A. Rosenfeld, J. Krüger, J. Bonse. Area dependence of femtosecond laser-induced periodic surface structures for varying band gap materials after double pulse excitation, Appl. Surf. Sci. (2013) 278, 7–12

[14] S. He, J. JJ Nivas, A. Vecchione, M. Hu, and S. Amoruso, On the generation of grooves on crystallinesilicon irradiated by femtosecond laser pulses, Opt. Expr. 24 (2016) 3238-3247.

[15] G. D. Tsibidis, C. Fotakis, E. Stratakis, From ripples to spikes: A hydrodynamical mechanism to interpret femtosecond laser-induced self-assembled structures. Phys. Rev. B 92 (2015) 041405-1 - 041405-6.

[16] S. He, J. JJ Nivas, K.K. Anoop, A. Vecchione, M. Hu, R. Bruzzese, S. Amoruso, Surface structures induced by ultrashort laser pulses: Formation mechanisms of ripples and grooves. Appl. Surf. Sci. 353 (2015) 1214–1222.

[17] J.Bonse, J. Krüger, Pulse number dependence of laser-induced periodic surface structures for femtosecond laser irradiation of silicon. J. Appl. Phys. 108 (2010) 034903.

[18] J. Bonse, M. Munz, and H. Sturm, Structure formation on the surface of indium phosphide irradiated by femtosecond laser pulses. J. Appl. Phys. 97 (2005) 013538.

[19] O. Varlamova, M. Bounhalli, J. Reif, Influence of irradiation dose on laser-induced surface nanostructures on silicon, Appl. Surf. Sci. 278, 62-66 (2013).

[20] Varlamova and J. Reif, Evolution of Femtosecond Laser Induced Surface Structures at Low Number of Pulses near the Ablation Threshold, J. Laser Micro/Nanoeng. 8, 300-303 (2013)

[21] O. Varlamova, C. Martens, M. Ratzke, J. Reif, Genesis of femtosecond-induced nanostructures on solid surfaces, Appl. Opt. 53 (2014) I10-I15.

[22] Q. Zhan, Cylindrical vector beams: from mathematical concepts to applications, Adv. Opt. Photon. 1 (2009) 1-57.

[23] L. Marrucci, E. Karimi, S. Slussarenko, B. Piccirillo, E. Santamato, E. Nagali, and F. Sciarrino, Spin-to-orbital conversion of the angular momentum of light and its classical and quantum applications, J. Opt. 13 (2011) 064001-1 - 064001-13.

[24] J. JJ Nivas, S. He, A. Rubano, A. Vecchione, D. Paparo, L. Marrucci, R. Bruzzese, S. Amoruso, Direct Femtosecond Laser Surface Structuring with Optical Vortex Beams Generated by a q-plate, Sci. Rep. 5 (2015) 17929-1 - 17929-12.

[25] J. Ouyang, W. Perrie, O. J. Allegre, T. Heil, Y. Jin, E. Fearon, D. Eckford, S. P. Edwardson, G. Dearden, Tailored optical vector fields for ultrashort-pulse laser induced complex surface plasmon structuring, Opt. Express 23, (2015) 12562–12572.

[26] K. K. Anoop, A. Rubano, R. Fittipaldi, X. Wang, D. Paparo, A. Vecchione, L. Marrucci, R. Bruzzese, S. Amoruso, Femtosecond laser surface structuring of silicon using optical vortex beams generated by a q-plate, Appl. Phys. Lett. 104 (2014) 241604-1 - 241604-5.

[27] K. K. Anoop, R. Fittipaldi, A. Rubano, X. Wang, D. Paparo, A. Vecchione, L. Marrucci, R. Bruzzese, S. Amoruso, Direct femtosecond laser ablation of copper with an optical vortex beam. J. Appl. Phys. 116 (2014), 113102-1 - 113102-9.

[28] O.J. Allegre, Y. Jin, W. Perrie, J. Ouyang, E. Fearon, S.P. Edwardson, and G Dearden, Complete wavefront and polarization control for ultrashort-pulse laser microprocessing, Opt. Express 21, (2013) 21198–21207.

[29] Y. Jin, O. J. Allegre, W. Perrie, K. Abrams, J. Ouyang, E. Fearon,S. P. Edwardson, and G. Dearden, Dynamic modulation of spatially structured polarization fields for real-time control of ultrafast laser-material interactions, Opt. Express 21 (2013) 25333–25343.

[30] K. Lou, S.-X. Qian, X.-L. Wang, Y.Li, B. Gu, C. Tu, H.-T. Wang, Two-dimensional microstructures induced by femtosecond vector light fields on silicon, Opt. Express 20 (2012) 120–127.

[31] M. Liu, Simple technique for measurements of pulsed Gaussian-beam spot sizes, Opt. Lett. 7 (1982) 196.

[32] J. JJ Nivas, S. He, K.K. Anoop, A. Rubano, R. Fittipaldi, A. Vecchione, D. Paparo, L. Marrucci, R. Bruzzese, S. Amoruso, Laser ablation of silicon induced by a femtosecond optical vortex beam, Opt. Lett. 40 (2015) 4611-4614.

[33] M. Huang, F. Zhao, Y. Cheng, N. Xu, Z. Xu, Origin of Laser-Induced Near-Subwavelength Ripples: Interference between Surface Plasmons and Incident Laser. ACS Nano 3 (2009) 4062–4070.

[34] Y. Han, S. Qu, The ripples and nanoparticles on silicon irradiated by femtosecond laser. Chem. Phys. Lett. 495 (2010) 241–244.

[35] G. D. Tsibidis, M. Barberoglou, P. A. Loukakos, E. Stratakis, C. Fotakis, Dynamics of ripple formation on silicon surfaces by ultrashort laser pulses in subablation conditions, Phys. Rev. B 86 (2012) 115316-1 - 115316-14.

[36] J. Reif, O. Varlamova, S. Uhlig, S. Varlamov, and M. Bestehorn, On the physics of self-organized nanostructure formation upon femtosecond laser ablation, Appl. Phys. A 117, 179–184 (2014)

[37] L.V. Zhigilei, Z. Lin, and D.S. Ivanov, Atomistic Modeling of Short Pulse Laser Ablation of Metals: Connections between Melting, Spallation, and Phase Explosion, J. Phys. Chem. C 113 (2009), 11892–11906.

[38] A. Pereira, P. Delaporte, M. Sentis, Optical and morphological investigation of backward-deposited layer induced by laser ablation of steel in ambient air, J. Appl. Phys. 98 (2005) 064902-1 - 064902-8.

J. JJ Nivas, et al., Femtosecond laser surface structuring of silicon with Gaussian and optical vortex beams, Appl. Surf. Sci. 418 (2017) 565–571, http://dx.doi.org/10.1016/j.apsusc.2016.10.162